Estimating Annual Global Upper Ocean Heat Content Anomalies Despite Irregular In Situ Ocean Sampling[*,**]

JOHN M. LYMAN[1,2] AND GREGORY C. JOHNSON[2]

[1] *Joint Institute for Marine and Atmospheric Research, University of Hawaii*

[2] *NOAA/Pacific Marine Environmental Laboratory, Seattle, Washington*

Submitted to *Journal of Climate*

26 September 2007

Revised

10 April 2008

Corresponding author address:

John M. Lyman, Pacific Marine Environmental Laboratory, NOAA/R/PMEL, 7600 Sand Point Way, Seattle, WA 98115 (email:John.Lyman@noaa.gov)

* Pacific Marine Environmental Laboratory Contribution Number 3123

** Joint Institute for Marine and Atmospheric Research contribution Number 07–367.

ABSTRACT

The effects of irregular in situ ocean sampling on estimates of annual globally integrated upper Ocean Heat Content Anomalies (OHCA) are investigated for sampling patterns from 1955 to 2006. An analytical method is presented for computing the effective area covered by an objective map for any given in situ sampling distribution. To evaluate the method, appropriately scaled sea surface height (SSH) anomaly maps from Aviso are used as a proxy for OHCA from 1993 to 2006. Use of these proxy data demonstrates that the simple area integral (SI) of such an objective map for sparse data sets does not agree as well with the actual integral as the weighted integral (WI), defined as the simple integral weighted by the ratio of the total area over the "observed" area. From 1955 to 1966, in situ ocean sampling is inadequate to estimate accurately annual global integrals of the proxy upper OHCA. During this period, the SI for the sampling pattern of any given year underestimate the 13-year trend in proxy OHCA from 1993 to 2006 by around 70%, and confidence limits for the WI are often very large. From 1967 to 2003 there appear to be sufficient data to estimate annual global integrals. Limited by the constraints of this analysis, the SI for any given year's sampling pattern still underestimate the 1993 to 2006 13-year trend in the proxy by around 30%, but the WI match the trend well with small confidence limits. For 2004 through 2006 in situ sampling, with near-global in situ Argo data coverage, the 1993–2006 13-year trend in the proxy is equally well represented by the SI or WI.

1. Introduction

Most of the Earth's warming signal arising from anthropogenic climate change is thought to reside in the upper ocean (Hansen et al. 2005; Levitus et al. 2005). To understand past and present global warming trends, and so to provide data for improvement of predictions of future changes, it is necessary to refine estimates of global upper Ocean Heat Content Anomalies (OHCA) and their uncertainties. Here the effect of the irregular sampling of the world's ocean over the last half-century on annual global OHCA estimates is quantified, and a different method of integration that may improve those estimates is proposed.

There are several ways to compute the global integral of mapped in situ data (Wunsch et al. 2007; Gille 2008). Two of them are compared here. One of these is a straightforward area integral of objectively mapped data. Because objective maps relax back toward the mean in data-sparse regions, this method generally assumes zero anomalies in regions that are not sampled. It will be referred to as the simple integral (SI) throughout this paper. The second method can be thought of as a weighted area integral only over regions with good data coverage weighted by the fraction of the ocean used where there are observations. This method assumes that the spatial mean of the anomalies in the unsampled regions is the same as the mean for the sampled regions. It will be referred to as the weighted integral (WI) throughout the paper.

Irregular historical in situ sampling of the oceans in both space and time complicates model/data comparisons. For instance, the variability in the global integral of upper OHCA depends on how data-poor regions are treated when integrating. It

turns out that the SI of objective maps have different variability than the WI (Gregory et al. 2004; AchutaRao et al. 2006; Gille 2008), making it difficult to validate the warming signal in a given model by comparing globally integrated model OHCA products to the SI of data-based OHCA maps. Furthermore, local regional trends in OHCA are large and variable, with some regions cooling for a time while other regions warm (e.g., Harrison and Carson 2007). Because of this small-scale variability in the decadal trends, the WI assumption that the trend in sampled regions is the same as in unsampled regions only holds on larger scales and not on regional scales. This variability, combined with sparse data coverage, has led some to conclude that historical data may not be sufficient to discern a global warming trend (Harrison and Carson, 2007).

One method used to improve comparisons of models with existing data is to sample model output at the same locations and times where the actual ocean is sufficiently sampled (e.g., Gregory et al. 2004; AchutaRao et al. 2006; Pierce et al. 2006). In these comparisons subjective criteria have been used to select areas where the number of observations is deemed sufficient to make a comparison. The WI generated from observational data and identically sampled model output can significantly improve agreement in OHCA comparisons. These comparisons suggest that these models are doing a good job of simulating global ocean heat content increases that are primarily due to anthropogenic climate change.

In situ ocean observation-based estimates of the globally integrated OHCA time series are a useful model benchmark and an important diagnostic for changes in the Earth's climate system (Hansen et al. 2005; Levitus et al. 2005). Recently

observational estimates of the global integral of OHCA tend to be calculated as SI of objective maps (Willis et al. 2004; Levitus et al. 2005; Ishii et al. 2006). While the complexity and sophistication of these objective analyses varies, they nearly all have anomalies that relax toward zero in areas of sparse data coverage. The integrals of these maps are affected by this tendency. Here a method for computing the fraction of the "observed" area in an objective map is derived (Appendix A) from the scales and methods used in the mapping. The SI and WI are compared side by side. To quantify the effects of irregular sampling on these integrals delayed-mode Aviso satellite sea surface height (SSH) anomalies are scaled appropriately to produce a synthetic data-based proxy for the global upper OHCA record from 1993 through 2006. Satellite SSH fields are not truly global, have possibly undefined errors, and along with heat content, include signals from freshwater variations (Willis et al. 2004; Wunsch et al. 2007). Besides including freshwater variations and deep variability, satellite SSH fields also contain mass (bottom pressure) signals (Gill and Niiler 1973; Ponte 1999). These potential complications notwithstanding, the SSH maps constitute a useful, continuous, high-resolution, and nearly global observational record over the ice-free oceans that have been shown to be correlated with in situ upper OHCA observations (White and Tai 1995; Gilson et al. 1998; Willis et al. 2004). However, there are regions where the correlation is not strong (Figure 4 in Willis et al. 2004). For the purpose of this analysis, the synthetic estimate of OHCA from SSH is considered the complete global estimate of OHCA. The synthetic OHCA record from 1993 through 2006 is subsampled at the locations and time of the year that in situ data were collected for all years between 1955 to 2006 to see how yearly sampling patterns affect both the linear trend

in globally integrated OHCA from 1993 to 2006 and sampling errors on the global integrals during those years.

Applying these methods to sampling patterns for any year prior to 1993 indicates how well the historical sampling for that year would have performed in estimating the global integral and its trend over the 13 years of Aviso SSH. Trends in OHCA vary from decade to decade and location to location (Harrison and Carson 2007). These decadal changes make estimates of pre-1993 sampling errors likely to be only a rough approximation of the true sampling errors.

Here the focus is on how historical sampling of world oceans affects global annual OHCA values and their errors along with developing and evaluating an appropriate scheme for constructing the WI of OHCA maps from in situ data. The scheme derived here estimates the effective area or "observed" area used in the WI from the scales and methods used in the mapping. Hence the effective area is estimated from the mapping procedures used, rather than using a subjective selection criteria such as the number of observations in a bin. Unknown, potentially large, and difficult to quantify instrument biases that may affect the SSH fields (Wunsch et al. 2007) are ignored. Possible errors in the covariance function and the climatology that could impact estimates of upper OHCA based on in situ data (AchutaRao et al. 2007; Wunsch et al. 2007) are also ignored.

The data used to define the in situ sampling distribution, the satellite SSH anomaly fields used as a proxy for upper OHCA, and the objective mapping techniques are discussed in section 2. The spatial and temporal structures of the data distribution are analyzed in section 3. The effects of irregular sampling are investigated in section 4

for 13-year trends and in section 5 for 3- to 13-year trends. An estimate of the sampling error on the global integral of OHCA is computed in section 6. The results are discussed and summarized in section 7.

2. Data and mapping

In situ ocean temperature measurements are a mixture of data mostly from reversing thermometers used at hydrographic stations, Mechanical BathyThermograph (MBT) profiles, eXpendable Bathythermograph (XBT) profiles, ship board conductivity-temperature-depth (CTD) profiles, moored buoy thermistor records (many from the Tropical Atmosphere Ocean array), and autonomous profiling CTD float data (primarily from Argo). The data used here were obtained from the World Ocean Database 2005 (Boyer et al. 2006), the Global Temperature & Salinity Profile Project (GTSPP), and the Argo Global Data Assembly Centers. Because of known but as yet not completely resolved biases among data from different instrument types (AchutaRao et al. 2007; Gouretski and Koltermann 2007; Wijffels et al. 2008; Willis et al. 2008), no attempt is made here to produce a heat content curve from in situ observations. Instead, the effects of irregular sampling are analyzed using a synthetic estimate of OHCA from sea surface height (SSH).

Nonetheless, the in situ data were subject to some basic quality control (QC) procedures to identify valid in situ data locations in the historical record. In order to remove duplicates between the different databases, profiles within 15 minutes in time and 3.6 arc seconds in space were removed from the GTSPP. This process was repeated twice. Profiles with insufficient vertical resolution were also discarded. To

have sufficient vertical resolution, the upper 400 m of the profiles were required to contain at least six data points flagged as good, a good measurement in the upper 30 m, a maximum good measurement depth exceeding 300 m, and depth spacing no more than twice that of the standard depths used in the World Ocean Database. Retained profiles were then subjected to further QC in World Meteorological Organization (WMO) squares. Squares with small numbers of profiles were combined. Then, by visual inspection, profiles with obviously spurious data compared to the bulk of the data in each square were discarded. Finally, OHCA estimates within these squares that fell outside of four standard deviations were discarded. The profiles that were left were considered good profiles, and SSH subsampled at their locations and times was used to estimate the depth-integrated OHCA in the upper 750 m.

Mapped satellite SSH anomaly estimates come from subsampled combined Aviso SSH. This product is an optimal merging of SSH from multiple platforms: Topex/Poseidon, Jason, ERS-1/2, and Envisat. The resulting product has 7-day temporal and approximately 150–200 km spatial resolution (Ducet et al. 2000). In this analysis SSH anomalies are used as a surrogate for upper ocean heat content anomalies by exploiting the strong correlations between SSH anomalies and available in situ estimates of OHCA (White and Tai 1995; Gilson et al. 1998; Willis et al. 2004; Lyman et al. 2006). These correlation coefficients vary geographically. However, here a global average regression coefficient of 51 ± 13 zeta-joules cm^{-1} is used (Lyman et al. 2006), where the error represents the spatial standard deviation.

Objective mapping (e.g., Wunsch 1996) covariance functions, correlation length scales, and signal-to-noise ratios used here follow those adopted by Willis et al. (2004)

and used again in Lyman et al. (2006). These techniques, functions, and values apply to both the objective maps generated from subsampled Aviso SSH fields and to the fraction of "observed" area computed for these maps (Appendix A). Following Willis et al. (2004), the record-length mean is removed from each location from the SSH fields. Then, the annual cycle, in this case based on quarterly means of the 1993–2006 anomalies of the Aviso SSH record, is removed. As with the in situ OHCA, removing the annual cycle based on quarterly means leaves some of the annual variability in the data, producing fields that are comparable to in situ observations. The resulting fields are then subsampled at the location and time of the year for a given year's in situ data sampling and grouped into 1-year bins centered on the middle of each year. These grouped data are then spatially mapped. The mapping is a simple objective map containing both a small scale (~100 km) and a large scale (~1000 km) in its covariance function (Willis et al. 2004). The correlation function used in the objective map also includes a signal to noise ratio along the diagonal, to account for unresolved geophysical variability at timescales less than a year and is based on the Zang and Wunsch (2001) spectra.

3. Data distribution

In situ upper ocean sampling has varied substantially both spatially and temporally over the last half-century. Between 1955 and 1966, the percentage of the "observed" ice-free upper ocean increased from near 20 to 40% (Fig. 1). With widespread XBT use starting in 1967, the fraction of the ocean represented in that year's annual map rose to 48%. This fraction continued to rise to around 75% during

the 1980s and 1990s as programs such as the World Ocean Circulation Experiment (WOCE) were implemented. WOCE spun down in the late 1990s, and the sampling area decreased to 63% by 2000. Some of this decrease may be eliminated for the last decade once data have made their ways from originators to the World Ocean Database, as there can be a multi-year lag for this process. In addition, efforts to gather historical data by NOAA's National Ocean Data Center have and should continue to help to increase data coverage in past years. The percentage of area sampled increases again after 2000 as more and more Argo autonomous profiling CTD floats begin reporting data in real time. For every succeeding year since 2004, as Argo has been approaching its target of global sampling with 3000 active floats (achieved by November 2007), the area sampled has been a record, with 89% coverage reached in 2006.

The method for computing the "observed" area (see Appendix A) takes into account the covariance functions, correlation length scales, and error energies used in the objective mapping described in Section 2. This method contrasts with the practice of using subjective criteria on a number of observations in an averaging bin to select bins with sufficient measurements for use in computation of a WI or other quantity. The data-based estimate of signal to noise ratio added to the diagonal of the correlation function results in a low area coverage in regions with few observations.

The spatial distribution of observations evolves with changing methods of data collection. In the pre-XBT era, here analyzed starting in 1955 and ending in 1966, the upper ocean was sparsely sampled. Most of the observations were concentrated near coastlines in the northern hemisphere (Fig. 2). As XBTs came into use, the spatial coverage dramatically increased from 1967 through 2003 (Fig. 3). For this period most

of the northern hemisphere is well sampled with contrasting sparse coverage in the southern hemisphere, where shipping lanes are more widely spaced. From 2004 through 2006, Argo profiling CTD float data provide a fairly even spatial distribution of data throughout most of the ice-free oceans for in situ OHCA estimates (Fig. 4).

Aviso SSH maps are available from 1993 through 2006. During this period in situ sampling of OHCA changed from primarily XBT data along shipping routes to more even global coverage by the autonomous profiling CTD floats of Argo. This change is evident in the standard deviation of the "observed" sampling areas for annual objective maps of in situ OHCA data during this time period (Fig. 5). Large sampling variations are evident south of about 40°S in the Pacific Ocean, and even further north in parts of the South Atlantic and Indian Oceans. The irregular and poor sampling in the Southern Ocean prior to Argo contributes to uncertainty of global OHCA integrals (AchutaRao et al. 2007; Gille 2008). For example, sparse and seasonally biased sampling in the Southern Ocean could corrupt the estimates of means and seasonal cycles, and thus annual OHCA estimates. While these are real and important problems, they are not investigated here nor do they affect the results presented here, as the Aviso SSH records used here as a proxy for OHCA are well resolved.

4. 13-year warming trends

The fully resolved synthetic SSH estimate of the upper OHCA curve has a warming trend of 0.9 ± 0.1 W m^{-2} from 1993 through 2006 (Fig. 6, grey line), as estimated by a linear fit. Here and throughout the paper, OHCA trends are estimated by linear fits and are normalized to the area of the earth (Levitus et al. 2005; Lyman et al.

2006). As mentioned in section 2, the synthetic estimate contains signals besides just upper OHCA (most obviously, changes in ocean mass), is likely an overestimate of the true warming of the upper ocean (Willis et al. 2004), and should not be taken as an accurate estimate of the actual ocean warming.

Trend errors are expressed as 95% confidence intervals of the slopes of the linear fits. All estimates of standard errors in this paper reflect statistical error due to how well a line fits a set of data or how closely integrals of subsampled synthetic OHCA can reproduce the integral of the whole map, and are therefore limited to the confines of the assumptions of this subsampling exercise. These limitations include uncertainties due to the fact that SSH contains variability other than Upper OHCA (as discussed above). Additionally, the time period over which the 13-year trend is estimated (1993 to 2006) contains different phases of known modes of interannual variability such as El Niño-Southern Oscillation (ENSO), the Southern Annular Mode (SAM), the Indian Ocean Dipole (IOD), the North Atlantic Oscillation (NAO), the Pacific Decadal Oscillation (PDO), the Atlantic Multidecadal Oscillation (AMO), and Arctic Oscillation (AO) than from sampling periods from which the trends are estimated (1955 to 2006). These uncertainties, along with possible unknown instrument biases that could affect the correlation between SSH and upper OHCA, would more than likely increase the estimate of the standard error shown in this paper.

To examine the effects of irregular sampling on the 13-year warming trend, the synthetic upper OHCA was subsampled at the in situ data locations from 1993 to 2006. The resulting data were mapped and then spatially integrated. When spatially integrating the subsampled global OHCA maps it is necessary to define the method of

computing a global integral (Appendix A). Two of the simplest choices are (1) the SI, where OHCA values are assumed to tend toward zero in locations and times where there are few measurements, and (2) a WI, where the values of OHCA in regions that are not "observed" are assumed to be the same as the global mean in the "observed" regions (Appendix A).

Both of the methods are able to produce a trend within the confidence intervals on the complete synthetic trend (Fig. 6). The SI underestimate the synthetic trend at 0.8 ± 0.1 W m^{-2} while the WI overestimate the synthetic trend at 1.0 ± 0.1 W m^{-2}. Neither trend estimate is significantly different from the trend for the fully resolved data set, but individually they barely agree with each other. While this assessment of how the in situ sampling from 1993 through 2006 reproduces the synthetic warming trend over that period is useful, it says little of how the different sampling eras and integration assumptions affect the estimates of the synthetic trend.

By subsampling every year of the 13-year synthetic upper OHCA like the data distribution for a given year, it is possible to construct a 13-year time series of annual upper OHCA estimates for that single year's sampling pattern. This subsampling strategy differs from the one just presented in that it yields an annual upper OHCA time series from 1993 through 2006 for each year's data distribution. The results can be used to estimate sampling errors for any given year and assess the two different methods for global integration of OHCA. Because this strategy depends only on knowing the sampling pattern for the year under study, it can be applied to assess errors associated with historical sampling for years before Aviso SSH was available. The estimates of the trend for historical sampling before 1993 are only applicable to the complete trend

in as much as the 1993 to 2006 period represents the time period in which the data were taken.

The SI for sparse historical sampling patterns generally produce underestimates of the actual 1993–2006 synthetic warming trend. For instance, the very sparse 1955 sampling pattern produces a very low, 0.1 ± 0.1 W m^{-2} (Fig. 7, upper panel), estimate of the 13-year synthetic warming trend from the SI. This estimate is only a small fraction of the complete synthetic warming trend of 0.9 ± 0.1 W m^{-2}. Even the much better sampling pattern for 1995 results in a SI for the 1993–2006 period that estimates a synthetic warming trend, 0.7 ± 0.1 W m^{-2} (Fig. 7, lower panel), that is significantly less than the complete synthetic trend.

In situ ocean sampling patterns for every year (but the last few years) of the last half century result in significant underestimates of the 1993–2006 synthetic warming trend using the SI (Fig. 8). In the pre-XBT area of sampling, 1955–1966, the warming estimates range from 10–50% of the complete synthetic trend. The fraction of the synthetic trend estimated from the SI increases slowly to about 75% of the complete synthetic trend from 1967–2003. It is not until the Argo array approaches sparse global coverage in 2004 that the synthetic warming trend estimated from the SI for that year's sampling pattern is within the 95% confidence interval of the complete synthetic warming rate. The 95% confidence interval for the synthetic linear trend estimated from the SI stays near ± 0.1 W m^{-2} for all of the 53 years of data coverage (Fig. 8, lower panel).

Estimates of the global synthetic warming trend in annual upper OHCA from the WI (Fig. 8, upper panel) are always within the confidence interval on the WI (Fig.

8, lower panel). For pre-1967 sampling patterns, the synthetic trend estimates from the WI oscillate noticeably about the complete synthetic estimate. For post-1967 sampling patterns the synthetic trend estimates are remarkably close to the complete synthetic trend. While the WI produces an estimate closer to the complete synthetic trend, the process of dividing by fraction of "observed" area (Appendix A) can significantly increase the 95% confidence intervals for that estimate (Fig. 8, lower panel). This increase is largest when the data coverage is sparsest. For instance, the 95% confidence intervals for the trend estimate from the WI for the 1955 sampling pattern are 7 times larger than the confidence intervals for the trend from the fully resolved data set. As the data coverage increases, the confidence interval on the synthetic trend estimated from the WI decreases, reaching twice the complete synthetic level in 1967 and finally approaching the complete synthetic level by the 1990s.

5. Three- to 13-year trends

The method of computing the integral also affects how well the historical in situ sampling patterns reproduce linear warming trends over intervals between 3 and 13 years. As for the 13-year trend, the fidelity and confidence intervals for warming trends over these shorter intervals are examined by subsampling the synthetic upper OHCA.

A composite of estimated synthetic trends is used to examine how well different timescales are reproduced during different eras of sampling. This analysis is performed by estimating the linear trend from different segments of the 1993–2006 13-year synthetic upper OHCA curve for each sampling pattern from 1955 to 2006. The shorter

the trend, the more estimates in a particular sampling distribution. The results of these fits are summarized by era (Figs. 9–10).

For all timescales, before the widespread use of the Argo floats (1955 to 2003), the WI are able to reproduce the complete synthetic trend within the confidence interval while the SI produce trends that are well below those values (Fig. 9). In the pre-XBT era, 1955 to 1966, the SI underestimates the complete synthetic trends by 0.6 to 0.7 W m^{-2} for all timescales (Fig. 9, upper panel). The WI during that same era only underestimates the complete synthetic trend by <0.1 W m^{-2}, well within 95% confidence intervals for the complete synthetic values. Unlike those for the trends produced from the SI, the confidence level on the trends from the WI is strongly dependent on timescale. At shorter timescales, 95% confidence limits are near 0.8 W m^{-2}, close to the complete synthetic 13-year warming trend of 0.9 W m^{-2}. At longer timescales the 95% confidence intervals for synthetic trends estimated from the WI approach 0.3 W m^{-2}.

As the sampling increases during the XBT era (1967 to 2003), the mean difference from the complete synthetic warming trend also decreases (Fig. 9, lower panel). The SI produce synthetic trends that are an underestimate of about 0.3 W m^{-2} at all timescales. These trends lie near the outside edge of the 95% confidence interval. In contrast, the linear synthetic trends produced from the WI during the XBT era match the complete synthetic trend within ±0.01 W m^{-2}, indicating that synthetic trends estimated from the WI are effectively the same as the complete synthetic trends. The means of the synthetic trends produced from the WI all lie well within the 95%

confidence intervals, which, as in the pre-XBT era, start out large (0.3 W m^{-2}) for shorter timescales but decrease to about 0.1 W m^{-2} for longer timescales.

When Argo provides near-global coverage (2004–2006), trends from the WI overestimate the complete synthetic trends by about 0.05 W m^{-2} for all timescales studied (Fig. 10). In contrast, synthetic trend estimates from the SI are underestimates by about 0.1 W m^{-2} for all timescales. For both methods of computing the integrals, the synthetic trends estimated by mapping subsampled data agree with the complete synthetic trends within 95% confidence intervals.

6. Sampling error

Sampling error is estimated from the standard deviation of the difference between complete synthetic values of annual globally integrated upper OHCA and estimates based on the SI or WI (Lyman et al. 2006). Because the data sets have been updated, a slightly more stringent QC has been employed, and 2 more years of delayed-mode Aviso data have been added since that study, the sampling errors presented here for the SI are slightly larger than those shown in Lyman et al. (2006). Sampling errors computed from the WI are less than those computed from the SI for most of the record (Fig. 11). The larger errors from the SI are a reflection of the large underestimates of the trends (see section 3).

Over both the pre-XBT and XBT eras, the SI produces sampling errors that are about twice those of the WI. The exception is 1955, when the noise introduced by use of the WI is larger than that introduced by the underestimated trend. From 2004 to 2006, as global coverage increases, the two estimates converge.

Sampling error decreases as the sampling area increases. Sampling error starts out high in 1955: 50 zeta joules for the SI and 60 zeta joules for the WI. As XBTs come into wide use after 1967 sampling errors level out near 20 zeta joules for the SI and 10 zeta joules for the WI. Finally, with the Argo array approaching its target of near-global sampling with 3000 profiling CTD floats, the different estimates of the sampling error overlap near 5 zeta joules in 2005 and 2006.

7. Discussion and conclusions

Irregular sampling of the Earth's oceans from 1955 to 2006 impacts estimates of interannual to decadal trends of global integrals of upper OHCA. The impact depends on the method used to estimate the global integrals. Integrals of annual maps made from an OHCA proxy between 1993 and 2006 using sampling patterns from a given year are computed using two different methods. Synthetic warming trends in the global integral of upper OHCA on timescales between 3 and 13 years are significantly underestimated using the SI but are consistently estimated within 95% confidence limits using the WI based on 1993–2006 Aviso SSH. From 2004 through 2006, as Argo approaches global coverage, the estimates of synthetic trends using either method with those years' sampling patterns converge and agree with the complete synthetic estimates within 95% confidence intervals.

For the spatial patterns observed in SSH from 1993 to 2006, there is not sufficient in situ data coverage before 1967 to estimate the global integral of synthetic upper OHCA, regardless of the method used to compute the spatial integral. For sampling patterns from this pre-XBT era, spatial integrals based on the SI grossly

underestimate the synthetic trend for 1993–2006 by 0.7 W m^{-2} or 70% (Fig. 8). On the other hand, the WI masks the complete synthetic trend by increasing the statistical error on the linear fit. This masking is seen in the increase in the 95% confidence interval to 0.6 W m^{-2}, or 66% of the synthetic slope, for the 1955 sampling pattern (Fig. 8). Given pre-XBT sampling patterns, neither of these methods is adequate to estimate the complete synthetic 13-year linear trend of 0.9 ± 0.1 W m^{-2}.

After the introduction of the XBT, but before Argo began providing global coverage (1967 to 2003), the sampling density increased and the errors on the synthetic trend decreased, so that the 95% confidence interval for the 13-year warming trend was about 0.1 W m^{-2} using either the SI or the WI. During this era, the SI significantly underestimates the 13-year synthetic trend by 0.3 W m^{-2} or 30% (Fig. 8). Conversely, the WI accurately reproduces the 13-year synthetic trend within the 95% confidence interval.

For the most recent sampling distribution (2004 to 2006), with Argo approaching the goal of near-global sampling, the annual global integral of OHCA is accurately estimated at all scales regardless of spatial integration method (Fig. 10). The WI tends to slightly (but statistically insignificantly) overestimate the trend by 0.07 W m^{-2} during the Argo sampling era. This slight discrepancy could be due to an overestimate of the error energy used in the objective maps or because under-sampled regions warmed at a slower rate than well-sampled regions.

Of the two methods for computing global integrals considered in this paper, the WI appear to produce more accurate estimates of the global integral of synthetic OHCA than the SI. This is not surprising, in that the WI assumes that unsampled regions of the

world's ocean warm at the same 13-year warming rate as the sampled regions. While this is clearly not true on small spatial scales or for times when the ocean is well sampled (2004 to 2006) (Harrison and Carson 2007), this assumption seems to hold on large spatial scales over decades (Levitus et al. 2000) and is consistent with analyses showing that the Southern Ocean, the largest undersampled area, has warmed since the 1950s (Gille 2002).

An additional infill experiment was performed on Argo data from 2004 to 2006 to determine how well the global integral matched the integral of OHCA over the Southern Ocean (the oceans south of 30°S). Using a climatology based on the World Ocean Database 2005 both the SI and WI were computed removing Argo data in the Southern Ocean (not shown). These results were compared to the SI over the whole Argo data set. As with the synthetic OHCA, the WI produced a more realistic value of the globally integrated OHCA than the SI.

These results suggest that the WI is the preferable method for estimating historical OHCA global integrals at annual timescales. However, it is important to remember that these results are based on how well in situ sampling reproduces trends in Aviso SSH anomalies, which are here scaled for use as a proxy for upper OHCA or over short timescales. It seems likely, for example, that the global integral of SSH includes a significant large-scale freshwater component in addition to thermosteric expansion (Wunsch et al. 2007). It is also conceivable that interannual variability in globally integrated OHCA may be underestimated by the SSHA proxy. If this were true, the statistical error in the 13-year trend from the WI would be disproportionately underestimated compared to the error on the 13-year trend computed from the SI.

While it may not be certain that the WI is preferable, it has been shown that the two integration methods can produce significantly different results, both of which should be used in examining historical trends in OHCA if for nothing more than to quantify the sensitivity of the estimates to different methods of computing global integrals.

Sampling errors from 1967 to 2006 are adequate to estimate synthetic trends in OHCA (Fig. 11). Prior to 1967, both methods produce large errors in globally integrated upper OHCA, reaching 60 zeta joules in 1955 with the WI. The errors computed from the WI are likely a more realistic representation of the synthetic sampling error than those from the SI, in that the errors computed from the WI come from the scatter about the complete synthetic value, whereas the errors from the SI are related to its underestimation of the synthetic warming trend.

In terms of the sampling errors, in situ sampling patterns from 1967 to 2006 appear to be adequate to estimate trends in globally integrated upper OHCA, especially if the WI is used for the pre-Argo years when coverage was not truly global. However, sampling errors are only one portion of the error budget. Biases in the mean climatology, variability not represented in the 1993–2006 synthetic OHCA, and instrument biases that are difficult to detect and quantify could be large (AchutaRao et al. 2007; Gouretski and Koltermann 2007; Willis et al. 2007; Wunsch et al. 2007). Currently the structure of the globally integrated OHCA curve is uncertain, primarily due to an apparent temporal bias in the eXpendable BathyThermograph (XBT) data (Gouretski and Koltermann 2007) that is plausibly owing to temporal variations in XBT fall rates (Wijffels et al. 2008), along with a correctable error in about 7% of the Argo

profiling floats (Willis et al. 2007; 2008). It appears that rectification of these biases will act to reduce interannual variability in the OHCA curve, but the best corrections may not yet be established. For these reasons, an in situ estimate of the global integral of OHCA is not computed here.

Acknowledgments. Altimeter products used herein were produced by SSALTO/DUACS as part of the Environment and Climate EU Enact project (EVK2–CT2001–00117) and distributed by Aviso, with support from CNES. The bulk of the in situ data used herein was provided through the World Ocean Database 2005 and the Global Temperature-Salinity Profile Program (http://www.nodc.noaa.gov). Float data were collected and made freely available by Argo (a pilot program of the Global Ocean Observing System) and contributing national programs (http://www.argo.net/). Carl Wunsch, Bruce Cornuelle, Josh Willis, and three anonymous reviewers provided helpful comments. The NOAA Climate Program Office and the NOAA Office of Oceanic and Atmospheric Research provided support for this research. The findings and conclusions in this article are those of the authors and do not necessarily represent the views of the National Oceanic and Atmospheric Administration.

APPENDIX A

Two global integrals

An ideal global integral can be defined as $\sum_{\substack{i=0,I \\ j=0,J}} true_{i,j} dA_{i,j} = I_t$, where I_t is the true integral, and $true_{i,j}$ the true value that represents the area $dA_{i,j}$ at a location i, j. The true field can be separated into a spatial mean and anomaly, $true_{i,j} = true'_{i,j} + m_t$, calculated over A, the area of the ocean and $true'_{i,j}$ are the spatial anomalies relative to a true spatial mean, m_t, such that $\sum_{\substack{i=0,I \\ j=0,J}} true'_{i,j}\, dA_{i,j} = 0$. Hence,

$$I_t = m_t A, \tag{A1}$$

where m_t is estimated from the set of k observations, obs_k.

Given the spatial distribution of obs_k an objective mapping (e.g., Wunsch 1996) can be defined, $\langle obs_k \rangle_{i,j}$, where $\langle\ \rangle_{i,j}$ is an objective map to a location i, j. The spatial integral of the mapped observations is then,

$$I_o = \sum_{\substack{i=0,I \\ j=0,J}} \langle obs_k \rangle_{i,j} dA_{i,j}. \tag{A2}$$

a. Simple Integral (SI)

The simplest way to define a spatial integral is in terms of an area-weighted integral of the mapped observations or

$$I_t \approx I_o. \tag{A3}$$

This is equivalent to defining the spatial mean on the map grid as

$\langle obs_k \rangle_{i,j} \equiv \langle obs_k' \rangle_{i,j} + m_{map}$, such that $\sum_{\substack{i=0,I \\ j=0,J}} \langle obs_k' \rangle_{i,j} dA_{i,j} \equiv 0$ and m_{map} is the mean of the map. When substituted into (A2) these equations yield

$$m_{map} = \frac{I_o}{A}. \tag{A4}$$

If m_t is estimated by m_{map} then by substituting (A4) into (A1) yields (A3), the SI. This method intrinsically assumes that the data distribution is adequate to produce maps resolving the global integral.

b. Weighted integral (WI)

If correlation length scales used in the objective mapping are small compared to spatial scales of the gaps in the distribution of data, or if data are too few to overcome the noise to signal ratio used, the mapping will be inadequate in resolving the global integral. To circumvent this problem larger scales could be added to the correlation length scale; however there is no obvious physical basis for these additions, and they would lead to vastly larger matrices that would require significant computing resources to invert. An alternative option is to define a mean only where there are data, $obs_k = obs_k'' + m_{rep}$ such that, $\sum_{\substack{i=0,I \\ j=0,J}} \langle obs_k'' \rangle_{i,j} dA_{i,j} \equiv 0$, and m_{rep} is a representative spatial mean. Noting that m_{rep} is a spatial constant, (A2) can be rewritten as,

$$I_o = m_{rep} \sum_{\substack{i=0,I \\ j=0,J}} \langle 1_k \rangle_{i,j} dA_{i,j}, \tag{A5}$$

where $\langle 1_k \rangle_{i,j}$ is an objective map to location i, j where the data at positions k have been replaced by the value 1.

If m_t is estimated by m_{rep}, then by substituting (A5) into (A1) the true spatial integral can be estimated by the WI (a weighted version of the simple integral (A2)),

$$I_t \approx \frac{I_o A}{\sum_{\substack{i=0,I \\ j=0,J}} \langle 1_k \rangle_{i,j} dA_{i,j}}. \tag{A6}$$

The map

$\langle 1_k \rangle_{i,j}$ = the fractional "observed" area for a given data distribution, obs_k, (A7)

and

$$\frac{\sum_{\substack{i=0,I \\ j=0,J}} \langle 1_k \rangle_{i,j} dA_{i,j}}{A}, \tag{A8}$$

the weights, represent the fraction of the globe "observed".

(A8) is an objective way to estimate the fraction of the "observed" ocean used in a global integral. It is equivalent to only integrating the "observed" ocean and then scaling the result by the area of the whole ocean. As mentioned in the introduction, similar calculations have been done before. The difference here is that the "observed" area of the ocean is defined by the scales, error energies, and techniques used in the mapping.

Hence, changing the mapping techniques or parameters would alter the fraction of the observed ocean. In the case shown in the paper the correlation length scales and timescales are representative of the upper ocean. For deep variability it might be appropriate to increase these scales, which would result in an increase in the fraction of

the ocean observed. Additionally, it might be interesting to examine longer timescales, which would increase the number of observations in a given integral, also increasing the fraction of the ocean "observed". This exercise might result in an "observed" coverage that is adequate before 1967.

REFERENCES

AchutaRao, K., M. Ishii, B. D. Santer, P. J. Gleckler, K. E. Taylor, T. P. Barnett, D. W. Pierce, R. J. Stouffer, and T. M. L. Wigley, 2007: Simulated and observed variabilty in ocean temperature and heat content. *Proc. Nat. Acad. of Sci.*, **104,** 10 768–10 773.

AchutaRao, K. M., B. D. Santer, P. J. Gleckler, K. E. Taylor, D. W. Pierce, T. P. Barnett, and T. M. L. Wigley, 2006: Variability of ocean heat uptake: Reconciling observations and models. *J. Geophys. Res*, **111,** 20.

Boyer, T. P., J. I. Antonov, H. Garcia, D. R. Johnson, R. A. Locarnini, A. V. Mishonov, M. T. Pitcher, O. K. Baranova, and I. Smolyar, 2006: World Ocean Database 2005, Chapter 1: Introduction, NOAA Atlas NESDIS 60, S. Levitus Ed., U.S. Government Printing Office, Washington, D.C., 182 pp., DVD.

Ducet, N., P. Y. Le Traon, and G. Reverdin, 2000: Global high-resolution mapping of ocean circulation from TOPEX/Poseidon and ERS-1 and-2. *J. Geophys. Res*, **105,** 19 477–19 498.

Gill, A. E., and P. P. Niiler, 1973: The theory of the seasonal variability in the ocean. *Deep-Sea Res.,* **20**, 141–177.

Gille, S. T., 2002: Warming of the Southern Ocean since the 1950s. *Science*, **295,** 1275–1277.

Gille, S. T., 2008: Decadal-scale temperature trends in the southern hemisphere ocean. *J. Climate,* in press.

Gilson, J., D. Roemmich, B. Cornuelle, and L. L. Fu, 1998: Relationship of TOPEX/Poseidon altimetric height to steric height and circulation in the North Pacific. *J. Geophys. Res.*, **103,** 27 947–27 965.

Gouretski, V. V., and P. Koltermann, 2007: How much is the ocean really warming? *Geophys. Res. Lett.*, **37,** L01610, doi:10.1029/2006GL027834.

Gregory, J. M., H. T. Banks, P. A. Stott, J. A. Lowe, and M. D. Palmer, 2004: Simulated and observed decadal variability in ocean heat content. *Geophys. Res. Lett.*, **31,** L14614, doi:10.1029/2006GL026769.

Hansen, J., L. Nazarenko, R. Ruedy, M. Sato, J. Willis, A. Del Genio, D. Koch, A. Lacis, K. Lo, S. Menon, T. Novakov, J. Perlwitz, G. Russell, G. A. Schmidt, and N. Tausnev, 2005: Earth's energy imbalance: Confirmation and implications. *Science*, **308,** 1431–1435.

Harrison, D. E., and M. Carson, 2007: Is the world ocean warming? Upper-ocean temperature trends: 1950–2000. *J. Phys. Oceanogr.*, **37,** 174–187.

Ishii, M., M. Kimoto, K. Sakamoto, and S. Iwasaki, 2006: Steric sea level changes estimated from historical ocean subsurface temperature and salinity analyses *J. Oceanogr.*, **62,** 155–170.

Levitus, S., J. Antonov, and C. Stephens 2000: Warming of the world ocean. *Science*, **287,** 2225–2229.

Levitus, S., J. Antonov, and T. Boyer, 2005: Warming of the world ocean, 1955–2003. *Geophys. Res. Lett.*, **32,** L02604, doi:10.1029/2004GL021592.

Lyman, J. M., J. K. Willis, and G. C. Johnson, 2006: Recent cooling of the upper ocean. *Geophys. Res. Lett.*, **33,** L18604, doi:10.1029/2006GL027033.

Pierce, D. W., T. P. Barnett, K. M. AchutaRao, P. J. Gleckler, J. M. Gregory, and W. M. Washington, 2006: Anthropogenic warming of the oceans: Observations and model results. *J. Climate*, **19,** 1873–1900.

Ponte, R. M., 1999: A preliminary model study of the large-scale seasonal cycle in bottom pressure over the global ocean. *J. Geophys. Res.*, **104**, 1289–1300.

White, W. B., and C. K. Tai, 1995: Inferring interannual changes in global upper ocean heat storage from TOPEX altimetry. *J. Geophys. Res.*, **100,** 24 943–24 954.

Wijffels, S. E., J. K. Willis, C. Doingues, P. Barker, N. White, A. Gronell, K. Ridgeway, and J. Church, 2008: Changing eXpendable BathyThermograph fall rates and their impact on estimates of thermosteric sea level rise. *J. Climate,* in press.

Willis, J., J. M. Lyman, G. C. Johnson, and J. Gilson, 2007: Correction to "Recent cooling of the upper ocean". *Geophys. Res. Lett.*, **34,** L16601 doi:10.1029/2007GL030323.

——, 2008: In situ data biases and recent ocean heat content variability. *J. Atmos. Oceanic Tech.*, submitted.

Willis, J. K., D. Roemmich, and B. Cornuelle, 2004: Interannual variability in upper ocean heat content, temperature, and thermosteric expansion on global scales. *J. Geophys. Res.* **109,** 13, c12036, doi: 10.1029/2003JC002260.

Wunsch, C., 1996: *The Ocean Circulation Inverse Problem*, Cambridge University Press, pp. 442.

Wunsch, C., R. Ponte, and P. Heimbach, 2007: Decadal trends in sea level patterns: 1993–2004. *J. Climate,* **20**, 5889–5911.

Zang, X. Y., and C. Wunsch, 2001: Spectral description of low-frequency oceanic variability. *J. Phys. Oceanogr.*, **31,** 3073–3095.

FIGURE CAPTIONS

Figure 1. Percentage of global ice-free ocean sampled for in situ upper (0–750 m) Ocean Heat Content Anomaly (OHCA) for each calendar year defined by equation (A8).

Figure 2. Mean of annual "observed" area coverage computed from equation (A7) for years 1955 to 1966.

Figure 3. Mean of annual "observed" area coverage from 1967 to 2003.

Figure 4. Mean of annual "observed" area coverage from 2004 to 2006.

Figure 5. Standard deviation of annual "observed" area coverage from 1993–2006 based on 14 one-year maps.

Figure 6. Annual global integrals of synthetic OHCA in the upper 750 m estimated from Aviso SSH. When computed from the entire Aviso record (thick gray line) the OHCA curve has a linear trend of 0.9 ± 0.1 W m^{-2}, a linear trend of 0.8 ± 0.1 W m^{-2} when computed from the integrals of subsampled synthetic OHCA (thin dashed line), and a linear trend of 1.0 ± 0.1 W m^{-2} when computed from the WI of subsampled synthetic OHCA (thick dashed line). These curves are based solely on SSH and therefore do not reflect the true warming rate of the upper ocean.

Figure 7. Following Fig. 6, but for global OHCA integrals from the Aviso SSH record subsampled at 1955 (upper panel) and 1995 (lower panel) in situ data locations. For the 1955 data distribution the trend computed from the SI is 0.1 ± 0.1 W m^{-2} and 0.7 ± 0.7 W m^{-2} from the WI. For the 1995 data distribution the trend from the SI is 0.7 ± 0.1 W m^{-2} and 0.9 ± 0.1 W m^{-2} from the WI.

Figure 8. Summary of 13-year warming trends (upper panel) and their 95% confidence intervals (lower panel) plotted as a function of each year's data distribution from 1955 through 2006 for the entire synthetic estimates of OHCA (grey lines), the synthetic estimates computed from the SI (thin dashed lines), and the synthetic estimates computed from the WI (thick dashed lines). Only the confidence intervals for the entire synthetic estimate (lower panel) are shown in the upper panel.

Figure 9. Mean differences in the true linear trend and the trend computed from both the SI (thin dashed line) and the WI (thick dashed line) for 3- to 13-year timescales. Differences are averaged over all possible segments of the time series for sampling patterns from 1955 to 1966 (upper panel) and 1967 to 2003 (lower panel). Error bars are 95% confidence intervals.

Figure 10. Following Fig. 9 but for sampling patterns from 2004 to 2006.

Figure 11. Sampling error computed following Lyman et al. (2006) from synthetic estimates of globally integrated OHCA both for the SI (thin dashed line) and the WI (thick dashed line) for each year's data distribution.

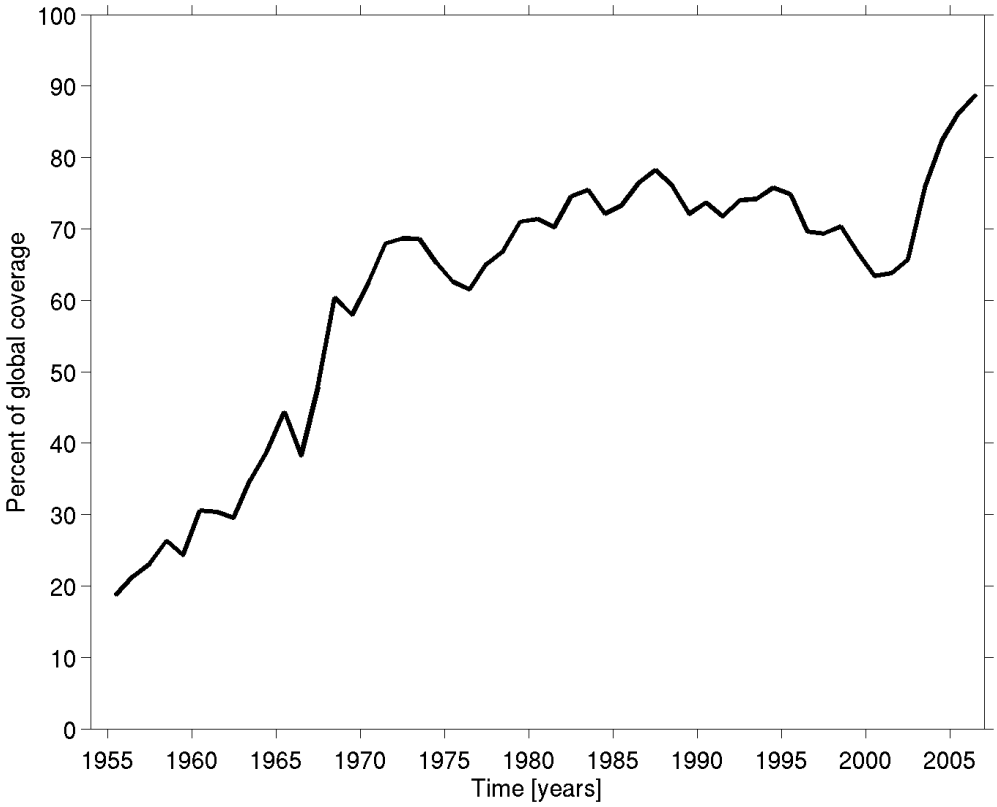

Figure 1. Percentage of global ice-free ocean sampled for in situ upper (0–750 m) Ocean Heat Content Anomaly (OHCA) for each calendar year defined by equation (A8).

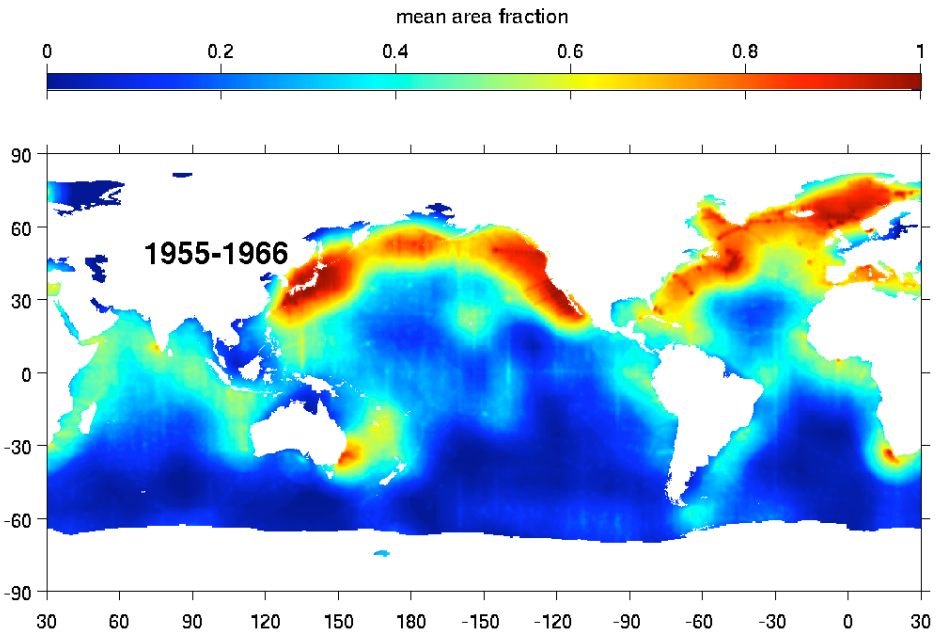

Figure 2. Mean of annual "observed" area coverage computed from equation (A7) for years 1955 to 1966.

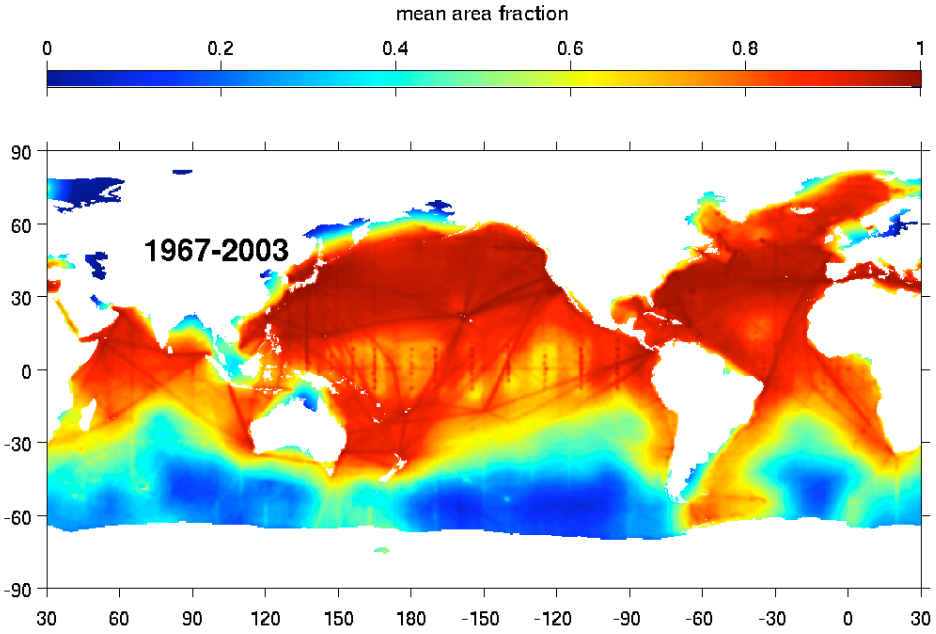

Figure 3. Mean of annual "observed" area coverage from 1967 to 2003.

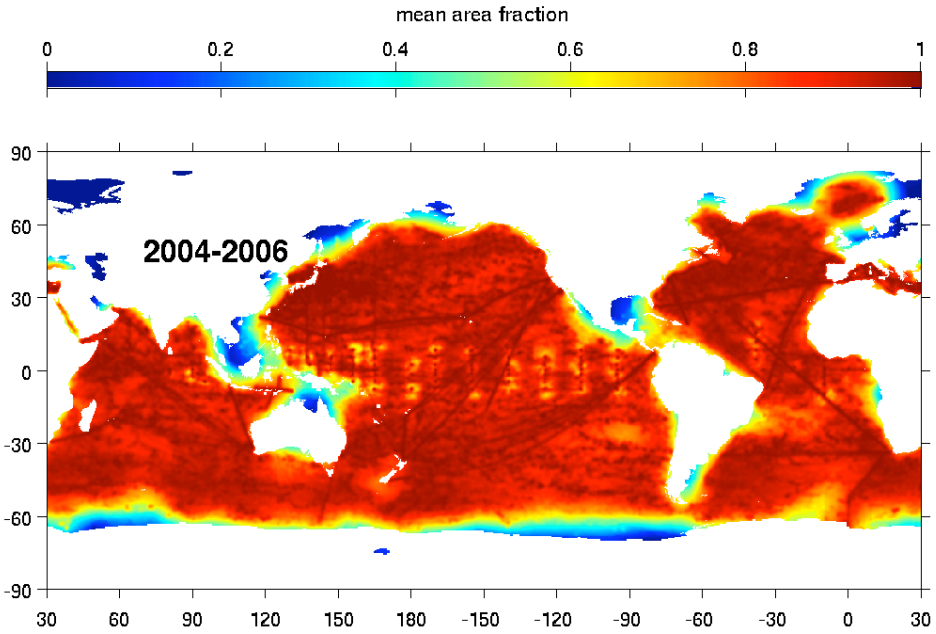

Figure 4. Mean of annual "observed" area coverage from 2004 to 2006.

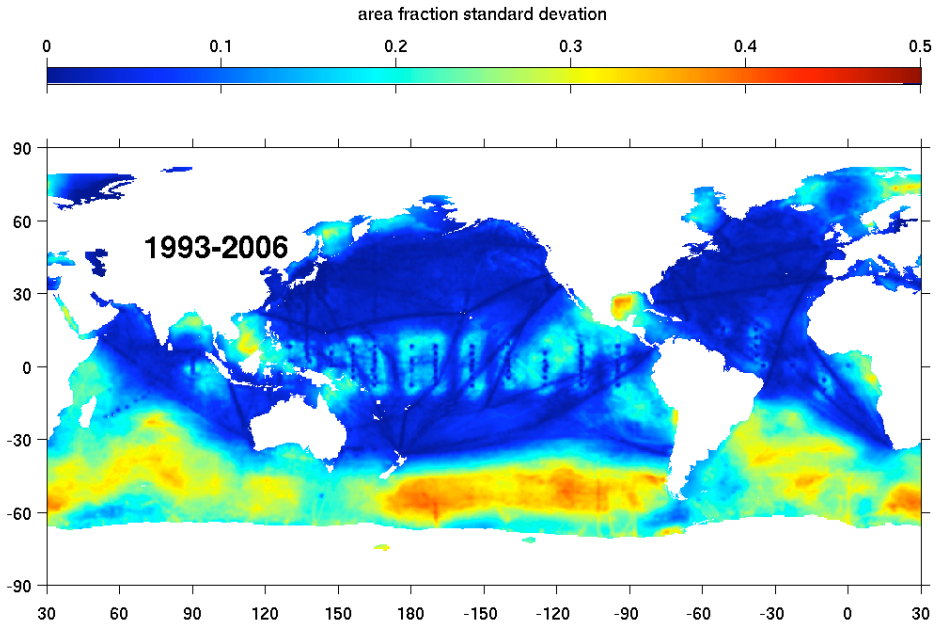

Figure 5. Standard deviation of annual "observed" area coverage from 1993–2006 based on 14 one-year maps.

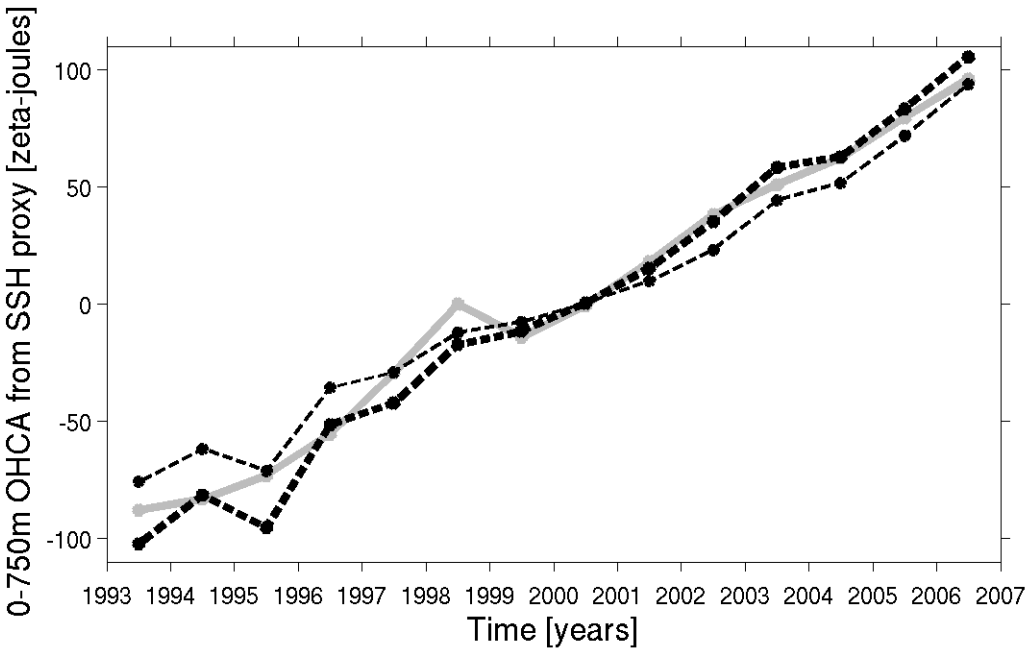

Figure 6. Annual global integrals of synthetic OHCA in the upper 750 m estimated from Aviso SSH. When computed from the entire Aviso record (thick gray line) the OHCA curve has a linear trend of 0.9 ± 0.1 W m^{-2}, a linear trend of 0.8 ± 0.1 W m^{-2} when computed from the integrals of subsampled synthetic OHCA (thin dashed line), and a linear trend of 1.0 ± 0.1 W m^{-2} when computed from the WI of subsampled synthetic OHCA (thick dashed line). These curves are based solely on SSH and therefore do not reflect the true warming rate of the upper ocean.

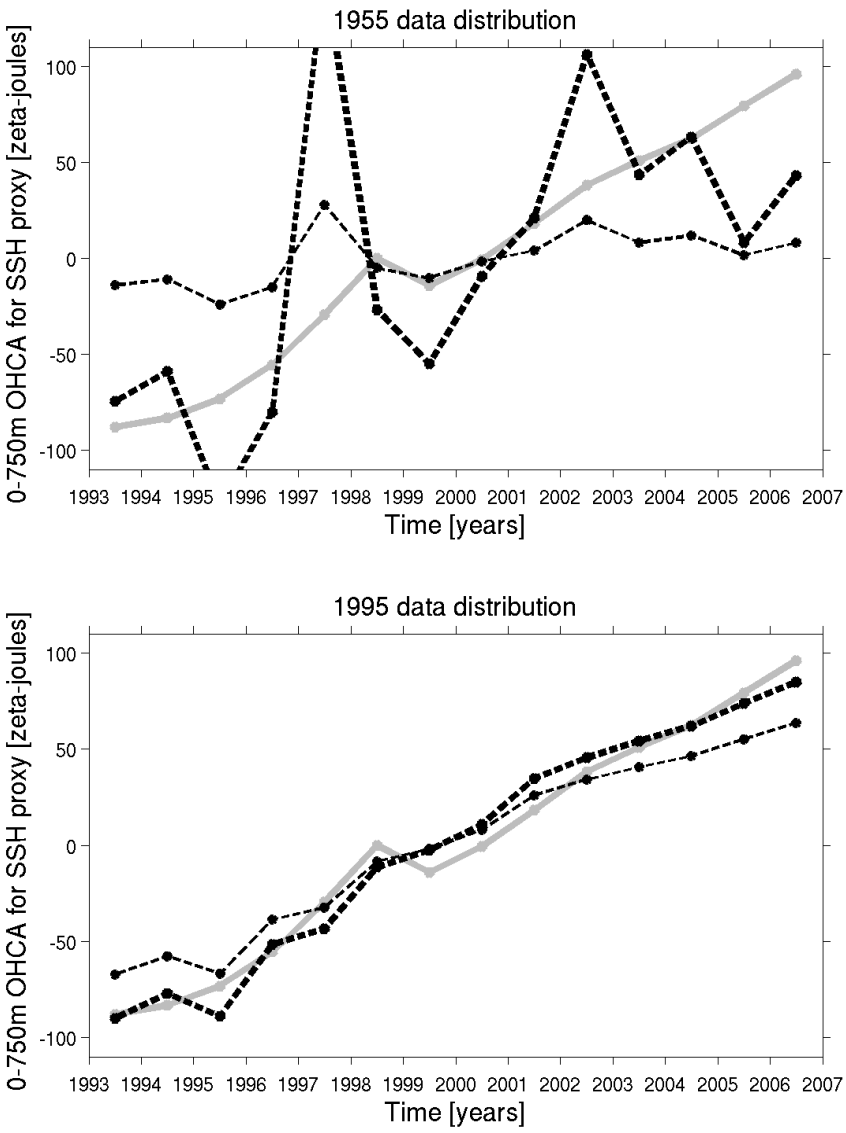

Figure 7. Following Fig. 6, but for global OHCA integrals from the Aviso SSH record subsampled at 1955 (upper panel) and 1995 (lower panel) in situ data locations. For the 1955 data distribution the trend computed from the SI is 0.1 ± 0.1 W m^{-2} and 0.7 ± 0.7 W m^{-2} from the WI. For the 1995 data distribution the trend from the SI is 0.7 ± 0.1 W m^{-2} and 0.9 ± 0.1 W m^{-2} from the WI.

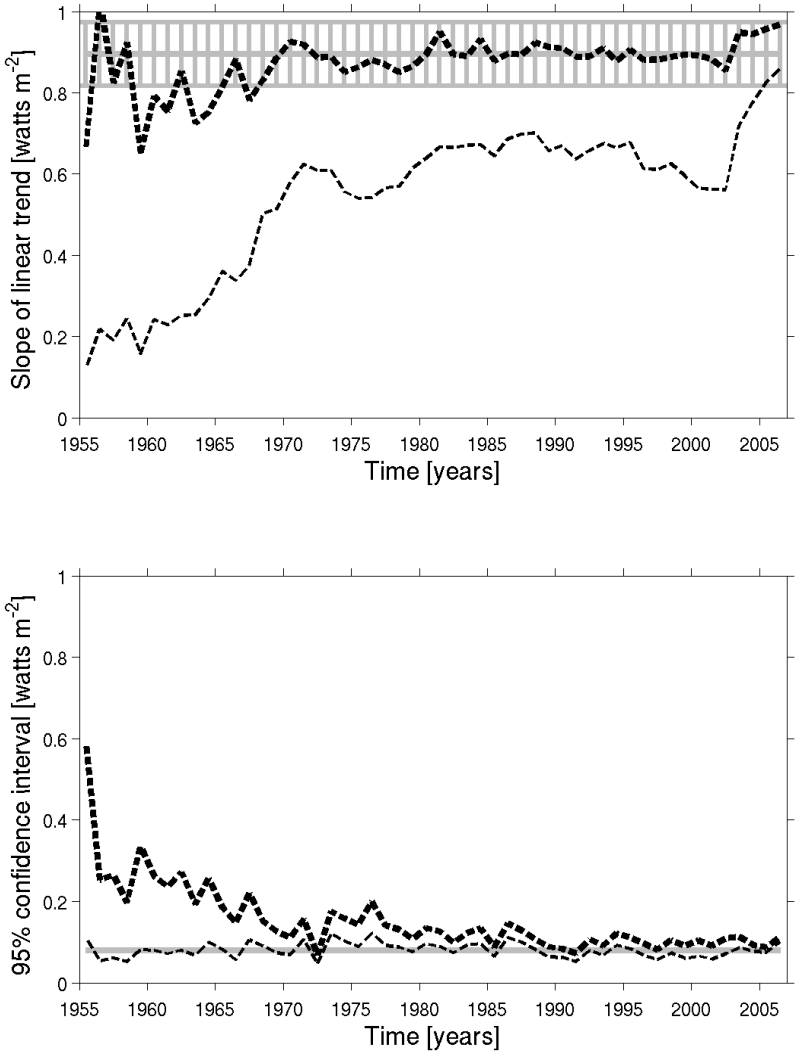

Figure 8. Summary of 13-year warming trends (upper panel) and their 95% confidence intervals (lower panel) plotted as a function of each year's data distribution from 1955 through 2006 for the entire synthetic estimates of OHCA (grey lines), the synthetic estimates computed from the SI (thin dashed lines), and the synthetic estimates computed from the WI (thick dashed lines). Only the confidence intervals for the entire synthetic estimate (lower panel) are shown in the upper panel.

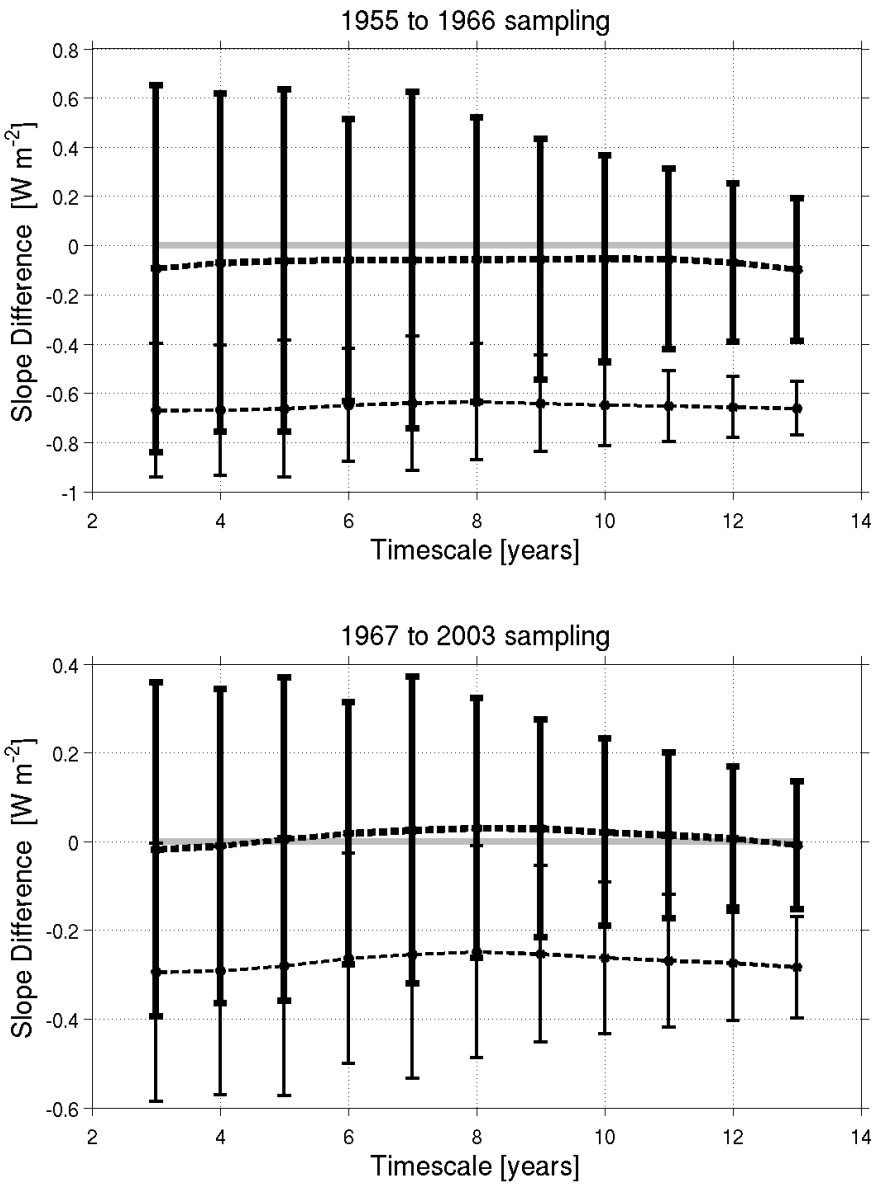

Figure 9. Mean differences in the true linear trend and the trend computed from both the SI (thin dashed line) and the WI (thick dashed line) for 3- to 13-year timescales. Differences are averaged over all possible segments of the time series for sampling patterns from 1955 to 1966 (upper panel) and 1967 to 2003 (lower panel). Error bars are 95% confidence intervals.

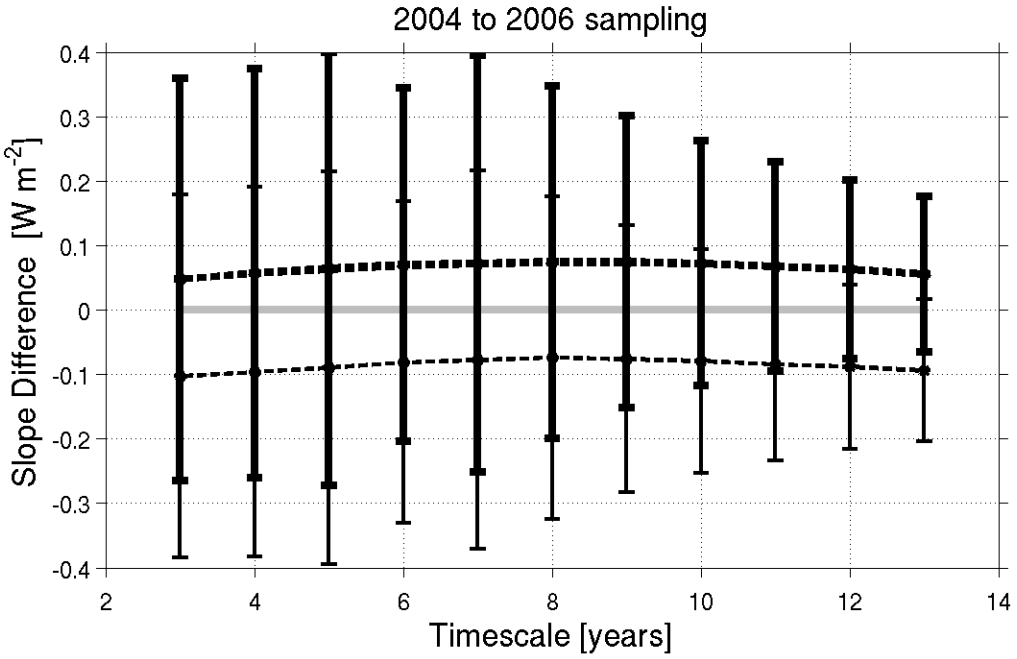

Figure 10. Following Fig. 9 but for sampling patterns from 2004 to 2006.

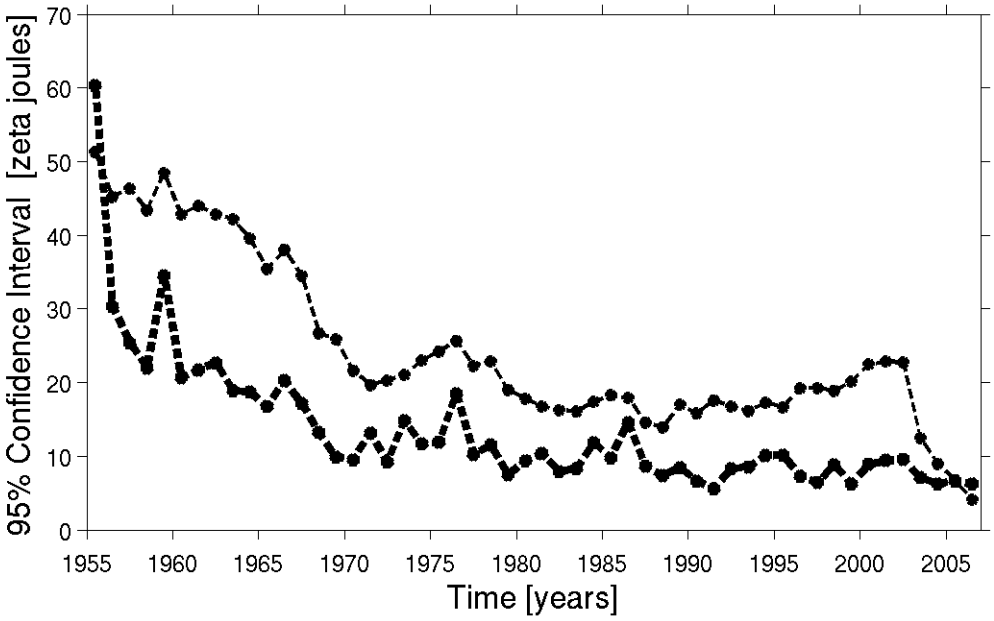

Figure 11. Sampling error computed following Lyman et al. (2006) from synthetic estimates of globally integrated OHCA both for the SI (thin dashed line) and the WI (thick dashed line) for each year's data distribution.